Kinetics controlled aging effect of ferroelectricity in Al-doped and Ga-doped $BaTiO_3$

Y. Y. Guo, M. H. Qin, T. Wei, K. F. Wang, and J.-M. Liu[a)]
Laboratory of Solid State Microstructures, Nanjing University, Nanjing 210093, People's Republic of China and International Center for Materials Physics, Chinese Academy of Sciences, Shenyang 110016, People's Republic of China

(Received 31 May 2010; accepted 28 August 2010; published online 17 September 2010)

Our experiments on ferroelectric aging of Al^{3+}- and Ga^{3+}-doped $BaTiO_3$ ceramics reveal the crucial role of migration kinetics of point defects (oxygen vacancies) besides the thermodynamic driving force based on the symmetry conforming short-range ordering scenario. The doping with Ga^{3+} or tiny Al^{3+} ions shows the clear aging effect, while the high-level Al^{3+}-doping suppresses the aging effect. The suppression is mainly attributed to the kinetically limited migration of oxygen vacancies due to the lattice shrinkage, while the other mechanisms may also make sense. © *2010 American Institute of Physics*. [doi:10.1063/1.3490700]

Ferroelectric (FE) aging effect has been observed in many oxide ferroelectrics.[1–4] This effect usually manifests itself as a spontaneous gradual change of the FE property with time at a given aging temperature (T). For example, for unpoled acceptor-doped FE systems, long time aging in FE state will lead to the reductions of dielectric and piezoelectric properties, abnormal double (or constricted) FE hysteresis (P-E) loop, and large electrostrain, due to the reversible domain switching mechanism.[5–10] Earlier works on Mn-doped $BaTiO_3$ single crystals and other materials have established the volume effect as one of the governing mechanisms, while other mechanisms associated with grain boundary effect or domain wall pinning may be also plausible.[5,7–10] Recent work of Ren group allows a symmetry conforming short-range ordering (SC-SRO) scenario of point defects as the microscopic origin of the volume effect.[10,11]

The volume effect refers to the formation and rearrangement of defect electric dipoles through the migration of point defects (typically oxygen vacancies, denoted as OVs). The proposed SC-SRO scenario provides the thermodynamic driving force.[10–13] The absence of aging effect in anion- or cation-donor doped ferroelectrics is considered to be caused by the kinetic suppression (immobile cation vacancies).[13] The OV migration from one site to one of its neighbors is implemented by oxygen ion motion to fill the vacancy.[14] Thus, a kinetic modulation of the FE aging effect becomes possible if one can kinetically control the migration of OVs, perhaps via route such as distorting the lattice. It is the major motivation of this work.

For example, one may dope 3+ ions at Ti^{4+} sites of $BaTiO_3$ (BT). The Al^{3+}-doping will result in the lattice shrinkage since Al^{3+} (ionic radius $r \sim 0.0535$ nm) is smaller than Ti^{4+} ($r \sim 0.0605$ nm),[15] and meanwhile OVs are created to satisfy the requirement of the charge neutrality. One may also dope Ga^{3+} ions ($r \sim 0.062$ nm),[15] generating OVs without lattice shrinkage. Given the efficiency of the kinetic modulation mentioned above, one would expect to observe different aging phenomena for Ga^{3+}-doped BT and heavily Al^{3+}-doped BT. In this work, we will investigate the aging behavior of Al^{3+}- and Ga^{3+}-doped BT ceramics. The time-dependent variations of P-E loops and activation energy for the OVs migration will be investigated, in order to unveil the crucial role of the kinetic modulation in competition with the thermodynamic driving force.

$Ba(Ti_{1-x}Al_x)O_3$ (BT-Al) and $Ba(Ti_{1-x}Ga_x)O_3$ (BT-Ga) samples were synthesized by the conventional solid-state reaction route, and $Ba(Ti_{1-x}Mg_x)O_3$ (BT-Mg) ceramics were also prepared for comparison study. All samples were sintered at 1300 °C for 6 h in air with several intermediate grindings. The structural characterizations using x-ray diffraction (XRD) with Cu Kα radiation at room temperature were performed. For electrical measurements, gold electrodes were sputtered on sample surfaces. All the samples were held at 300 °C for 4 h for deaging, followed by air-quenching down to room temperature to obtain the unaged (fresh) samples. To obtain the aged samples, the fresh samples were kept at 70 °C (slightly below the Curie point T_C for the most heavily doped sample) for different times (unit in day) and then cooled down to room temperature. This is the aging process. The P-E loops were measured using the RT6000HVS standard ferroelectric testing unit at room temperature and the impedance measurements were performed with HP4294A impedance analyzer.

Figure 1 gives the measured XRD patterns. All samples

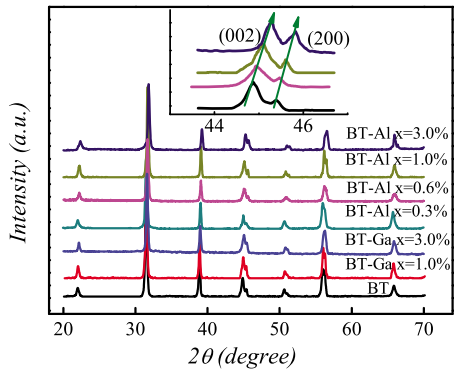

FIG. 1. (Color online) XRD patterns for all the samples. The inset shows the diffraction peaks of (002) and (200) planes for BT-Al at x=0, 0.6%, 1.0%, and x=3.0% from bottom to top, respectively.

[a)]Author to whom correspondence should be addressed. Electronic mail: liujm@nju.edu.cn.

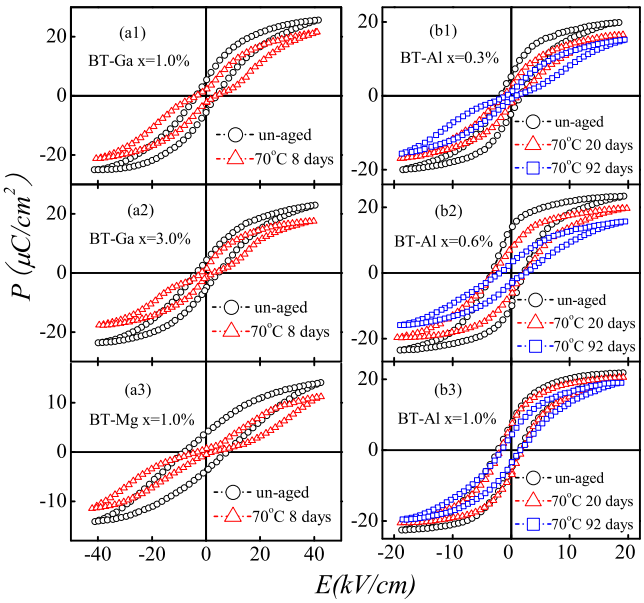

FIG. 2. (Color online) Measured *P-E* hysteresis loops at room temperature for several selected samples in the unaged (fresh) state and aged states: (a1) BT-Ga $x=1.0\%$, (a2) BT-Ga $x=3.0\%$, (a3) BT-Mg $x=1.0\%$, (b1) BT-Al $x=0.3\%$, (b2) BT-Al $x=0.6\%$, and (b3) BT-Al $x=1.0\%$. The time (day) and temperature (70 °C) for the aging of each sample are labeled, respectively, in each plot.

do have a single tetragonal structure and excellent crystallinity without second phase within the apparatus resolution. In comparison with BT itself, the slight right-ward shift of diffraction peaks for BT-Al at $x \geq 0.6\%$, as identified in the inset, indicates the lattice shrinkage. This is reasonable owing to the small ionic radius of Al^{3+}. No obvious shift for other doped samples can be detected, noting that Ga^{3+} has the similar size as Ti^{4+}.

Then we address the *P-E* loops for fresh and aged BT-Al, BT-Ga, and BT-Mg samples. All the unaged (fresh) samples show the normal single *P-E* loops, as shown in Fig. 2, while significant variations of the loops are identified after the aging. First of all, for BT-Ga at $x=1.0\%$ and 3.0%, double *P-E* loops are well developed after the aging only for eight days (under a high $E=40$ kV/cm), and this double-loop feature becomes more significant with increasing x [Figs. 2(a1) and 2(a2)]. Figure 2(b1) presents the *P-E* loops for BT-Al at $x=0.3\%$, showing the gradual loop-shrinking along the *P*-axis with increasing aging time (under a low $E=19$ kV/cm). By contrast, the loops for BT-Al at $x=0.6\%$ under $E=19$ kV/cm show no shrinking even by aging for 92 days [Fig. 2(b2)], in spite of slightly reduced *P*. For BT-Al at $x \geq 1.0\%$, the 92 days aged samples show almost the same loops as those of the fresh sample. In addition, for the sake of reference, we present in Fig. 2(a3) the fully developed double-loop under $E=40$ kV/cm for BT-Mg at $x=1.0\%$ which was aged only for eight days. These results allow us to conclude that the FE aging effect is remarkable in both BT-Ga and BT-Mg, but for BT-Al, no more trace can be detected at $x > 0.3\%$ under the identical aging conditions.

To understand these variations, one may consult to those possible underlying mechanisms. First, we look into the SC-SRO scenario for the volume effect. For all acceptor-doped samples in unaged states, the distribution of OVs follows the cubic symmetry and the six equivalent sites of oxygen octahedral are randomly occupied by OVs, while the lattice structure evolves into the polar tetragonal symmetry, generating the mismatching between the lattice symmetry itself and the distribution symmetry of OVs (defect symmetry).[10,11] This mismatching thus provides the driving force for the transformation of the defect distribution symmetry into the tetragonal one via the local migration of OVs among the six corners of oxygen octhedra.[10,11] The aging slightly below T_C assists in such a transformation. However, such assistance depends on the thermal-activation energy for the OVs diffusion in the lattice. The doping may influence the OVs migration and change the activation energy by distorting the lattice.[14] The simple physics is that the FE aging will not be possible unless both this driving force and the kinetic preference for the OVs migration are satisfied.

If this volume effect applies to the BT-Ga samples, it is reasonable to expect the significant FE aging effect in BT-Ga ($x=1.0\%$ and 3.0%), as confirmed in our experiments. During the aging, the distribution symmetry of OVs tends to match with that of the lattice. After the aging, the OVs become no longer mobile even driven by electric field *E*. During the *P-E* loop measurement, application of field *E* switches the FE domains but these OVs remain frozen in the original sites because of their immobility. This is a metastable state, because a thermodynamic restoring force provided by the associated defect electric dipoles is available, which reverses the switched FE domains upon the removal of *E*.[10] Therefore, the peculiar double-loop can be observed for the aged BT-Ga.

However, for BT-Al, the physics becomes more complicated. The density of OVs increases and the lattice shrinks with *x*, since Al^{3+} is smaller than Ti^{4+}. The shrinking effect would affect the migration of OVs and the matching of the distribution symmetry of OVs with the lattice symmetry, i.e., the distribution of OVs reserves the cubic symmetry although the lattice takes the polar tetragonal symmetry. This suppression becomes more serious at higher *x*. In consequence, for highly doped samples, the FE aging effect may be thermodynamically preferred but kinetically completely blocked.

Along this line, we perform additional experiment by checking the FE aging effect of BT-Mg at $x=1.0\%$. Because Mg^{2+} ($r \sim 0.072$ nm) is larger than Ti^{4+},[15] this doping will expand the lattice. Considering the different aging phenomena between Ga^{3+}-doped BT and heavily Al^{3+}-doped BT mentioned above, one would expect that the OV diffusion might be easier in the expanded lattice, benefiting to the FE aging effect. In fact, our results [Fig. 2(a3)] confirm that the aging effect of this sample is more remarkable than that of BT-Ga at $x=3.0\%$ under the same aging conditions.

Backing on these data and the volume effect such as the SC-SRO scenario, we argue that the migration kinetics of OVs becomes crucial in controlling the FE aging effect. Given that the diffusion process of OVs is mainly thermally activated, more evidence on the aging effect is available by evaluating the dependence of activation energy on *x*. For perovskite ferroelectrics, the dc conductivity σ_{dc} is mainly attributed to the electromigration of OVs.[16] We employ the complex impedance spectroscopy to measure σ_{dc} satisfying $\sigma_{dc} \propto T^{-1}\exp(-E/k_BT)$, where *E* is the conductance activation energy, k_B the Boltzmann constant, and *T* the absolute temperature.[17–19] Figure 3 shows the measured data in the plot of $\ln(\sigma_{dc}T)$ versus $1000/T$ for all compositions. The

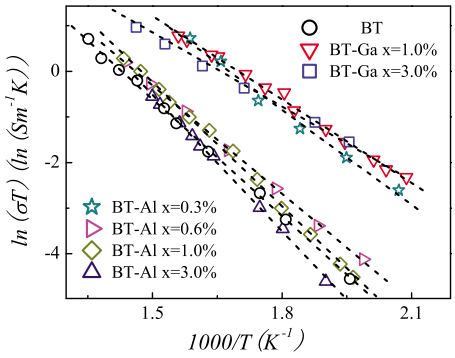

FIG. 3. (Color online) Arrhenius plot $\ln(\sigma_{dc}T)$ vs $1000/T$ for various samples as indicated.

dashed lines are the fitting results. The evaluated E are summarized in Table I and consistent with earlier reported values for perovskite oxides.[7,20,21] Clearly, the BT-Al has higher E than that of BT-Ga. Moreover, E of BT-Ga decreases slightly with increasing x, indicating kinetically easier migration for OVs. The evaluated $E \sim x$ trend is identical with other reports.[16,22] However, for BT-Al, E increases rapidly with increasing x, suggesting the kinetic suppression of the OVs migration. Therefore, all the observed FE aging behaviors are well explained in the volume effect framework.

What should be addressed is that other mechanisms responsible for the aging cannot be excluded in doped $BaTiO_3$ ceramics,[5,22] especially Al^{3+}-doped $BaTiO_3$, in spite of the qualitatively reasonable illustration by the volume effect, In fact, earlier work[7] on Al^{3+}-doped $Pb(Zr,Ti)O_3$ ceramics suggests that the grain boundary effect rather than the volume or wall effect is responsible for the observed FE aging behavior. It is claimed that during the aging, the intergranular second phase will collect space charges that can compensate the spontaneous polarization locally. The resulting space charge field is equivalent to an internal bias field which impresses an overall preferred direction of polarization on each crystallite. Returning to our work, although no Al^{3+}-rich second phase was observed in Al^{3+}-doped BT ceramics because of the very low concentration of Al^{3+}, the influence of the space charges gathered around the grain boundaries should be there. Thus, in Al^{3+}-doped BT ceramics, more than one mechanism may be active and responsible for the FE aging effect.

TABLE I. The activation energy of the estimated dc conductivity for all compositions.

Sample	E (eV)	Sample	E (eV)
BT	0.74 ± 0.01	BT-Al $x=0.3\%$	0.59 ± 0.03
BT-Ga $x=1.0\%$	0.50 ± 0.01	BT-Al $x=0.6\%$	0.68 ± 0.01
BT-Ga $x=3.0\%$	0.46 ± 0.02	BT-Al $x=1.0\%$	0.78 ± 0.02
		BT-Al $x=3.0\%$	0.86 ± 0.02

In conclusion, we have investigated the FE aging effects of Al^{3+}- and Ga^{3+}-doped BT ceramics. Given the aging at 70 °C, the Ga^{3+}-doped BT samples show clear aging effects, while such effects in Al^{3+}-doped BT are essentially suppressed at a level higher than 0.3%. It is argued that the underlying mechanism is that the Al^{3+}-doping induced lattice shrinkage would hinder the OVs migration. We propose the crucial and competitive role of the migration kinetics of OVs in modulating the FE aging effect, while the other mechanisms such as the grain boundary effect may also play some role in it.

The authors would like to acknowledge financial support from the National Natural Science Foundation of China (Grant Nos. 50832002 and 10874085) and the National Key Projects for Basic Researches of China (Grant Nos. 2009CB623303 and 2011CB922101).

[1]F. Jona and G. Shirane, *Ferroelectric Crystals* (Macmillan, New York, 1962).
[2]W. A. Schulze and K. Ogino, Ferroelectrics **87**, 361 (1988).
[3]B. Jaffe, W. R. Cook, and H. Jaffe, *Piezoelectric Ceramics* (Academic, New York, 1971).
[4]K. Uchino, *Ferroelectric Device* (Dekker, New York, 2000).
[5]P. V. Lambeck and G. H. Jonker, J. Phys. Chem. Solids **47**, 453 (1986).
[6]D. Damjanovic, Rep. Prog. Phys. **61**, 1267 (1998).
[7]K. Carl and K. H. Härdtl, Ferroelectrics **17**, 473 (1978).
[8]M. Takahashi, Jpn. J. Appl. Phys., Part 1 **9**, 1236 (1970).
[9]W. L. Warren, D. Dimos, B. A. Tuttle, R. D. Nasby, and G. E. Pike, Appl. Phys. Lett. **65**, 1018 (1994).
[10]X. Ren, Nature Mater. **3**, 91 (2004).
[11]X. Ren and K. Otsuka, Phys. Rev. Lett. **85**, 1016 (2000).
[12]D. M. Lin, K. W. Kwok, and H. L. W. Chan, Appl. Phys. Lett. **90**, 232903 (2007).
[13]H. X. Bao, L. X. Zhang, Y. Wang, W. F. Liu, C. Zhou, and X. B. Ren, Appl. Phys. Lett. **91**, 142903 (2007).
[14]J. Song, L. R. Corrales, G. Kresse, and H. Jonsson, Phys. Rev. B **64**, 134102 (2001).
[15]R. D. Shannon, Acta Crystallogr., Sect. A: Found. Crystallogr. **32**, 751 (1976).
[16]S. Steinsvik, R. Bugge, J. Gjonnes, J. Tafto, and T. Norby, J. Phys. Chem. Solids **58**, 969 (1997).
[17]M. J. Forbess, S. Seraji, Y. Wu, C. P. Nguyen, and G. Z. Cao, Appl. Phys. Lett. **76**, 2934 (2000).
[18]T. Wei, Y. Wang, C. Zhu, X. W. Dong, Y. D. Xia, J. S. Zhu, and J.-M. Liu, Appl. Phys. A: Mater. Sci. Process. **90**, 185 (2008).
[19]Y. Wang, Q. Y. Shao, and J.-M. Liu, Appl. Phys. Lett. **88**, 122902 (2006).
[20]S. H. Cha and Y. H. Han, J. Appl. Phys. **100**, 104102 (2006).
[21]C. Ang, Z. Yu, and L. E. Cross, Phys. Rev. B **62**, 228 (2000).
[22]M. I. Morozov and D. Damjanovic, J. Appl. Phys. **107**, 034106 (2010).